**Supplementary Table 1.** Association between PCPG subtype and metastasis (Fisher's exact test, Benjamini-Hochberg multiple testing correction)

| Subtype | n_metastatic | n_non-metastatic | odds_ratio | p.value | p.adjust |
|---|---|---|---|---|---|
| C1A1 (SDHx) | 23 | 31 | 8.5091868 | 7.77E-10 | 6.22E-09 |
| C1A2 (SDHx-HN) | 8 | 9 | 7.22947326 | 3.18E-04 | 8.47E-04 |
| C1B1 (VHL) | 8 | 69 | 0.79654021 | 0.70287852 | 0.70287852 |
| C1B2 (EPAS1) | 0 | 19 | 0 | 0.148234332 | 0.169410665 |
| C2A (Kinase) | 7 | 145 | 0.24517765 | 1.94E-04 | 7.76E-04 |
| C2B1 (MAX) | 2 | 48 | 0.27015295 | 0.065708259 | 0.087611012 |
| C2B2 (MAML3) | 4 | 9 | 3.33292785 | 0.062663338 | 0.087611012 |
| C2C | 1 | 48 | 0.13254447 | 0.018560746 | 0.037121492 |

**Supplementary Table 2.** IHC scoring in 12 PCPG and 2 normal adrenal tissues

| SampleID | ID Number | Subtype | Genotype | CD3 per 2mm$^2$ | CD68 per 2mm$^2$ | CD163 per 2mm$^2$ | CD206 per 2mm$^2$ |
|---|---|---|---|---|---|---|---|
| E041 | VPH36T | C1A1 (SDHx) | SDHA | 3 | 9 | 15 | 4 |
| E019 | VPH23T | C1A1 (SDHx) | SDHB | 6 | 18 | 40 | 12 |
| P018-PGL1 | P018P1.2.2 | C1A1 (SDHx) | SDHB | 5 | 42 | 50 | 9 |
| P018-PGL3 | P018M3 | C1A1 (SDHx) | SDHB | 1 | 12 | 70 | 55 |
| E024 | VPH35T | C1B1 (VHL) | VHL | 3 | 4 | 150 | 150 |
| E041 | 07SH0498 | C1B1 (VHL) | VHL | 5 | 60 | 250 | 240 |
| E042 | 18SH0221 | C1B1 (VHL) | VHL | 15 | 24 | 185 | 175 |
| E035 | 07AH0391 | C2A (Kinase) | HRAS | 3 | 44 | 150 | 125 |
| E017 | VPH20T | C2A (Kinase) | NF1 | 10 | 45 | 50 | 25 |
| E174 | 17NH0056T1 | C2A (Kinase) | NF1 | 1 | 2 | 25 | 12 |
| E007 | VPH08T | C2A (Kinase) | TMEM127 | 1 | 2 | 1 | 4 |
| E008 | VPH09T | C2B2 (MAML3) | UBTF-MAML3 | 5 | 3 | 120 | 25 |
| Normal 1 | Adrenal 22P5165 | NAM | Normal | 12 | 35 | 75 | 25 |
| Normal 2 | Adrenal | NAM | Normal | 4 | 30 | 150 | 95 |

**Supplementary Table 3.** Differentially expressed genes in metastatic PCPG compared to non-metastatic PCPG. Differential gene expression was determined by limma using empirical Bayes moderated t-statistics, and adjusted for FDR with Benjamini-Hochberg correction (BH adj. P-value < 0.05)

| Gene | logFC | AveExpr | t | P.Value | adj.P.Val | B | Pathways Groups | Comparison |
|---|---|---|---|---|---|---|---|---|
| JANSKY_cycling_neuroblast_genes | 0.6338 | 0.0156 | 4.82 | 2.10E-06 | 0.0001 | 4.5086 | Proliferation | metastatic_vs_nonmetastatic_in_C1A |
| HALLMARK_G2M_CHECKPOINT | 0.4212 | -0.0214 | 4.2722 | 2.46E-05 | 0.0008 | 2.1926 | Proliferation | metastatic_vs_nonmetastatic_in_C1A |
| ZETHOVEN_SCLCs | -0.442 | 0.0037 | -3.6199 | 0.0003 | 0.0075 | -0.233 | SCLCs | metastatic_vs_nonmetastatic_in_C1A |
| HALLMARK_MITOTIC_SPINDLE | 0.1859 | -0.057 | 3.0867 | 0.0022 | 0.0342 | -1.9378 | Proliferation | metastatic_vs_nonmetastatic_in_C1A |
| HALLMARK_E2F_TARGETS | 0.2718 | -0.0776 | 3.008 | 0.0028 | 0.0342 | -2.1677 | Proliferation | metastatic_vs_nonmetastatic_in_C1A |
| JANSKY_late_SCP_genes | -0.3055 | 0.0025 | -2.9814 | 0.0031 | 0.0342 | -2.2441 | SCLCs | metastatic_vs_nonmetastatic_in_C1A |
| HALLMARK_GLYCOLYSIS | 0.1594 | -0.0536 | 2.7989 | 0.0054 | 0.0498 | -2.7508 | Other | metastatic_vs_nonmetastatic_in_C1A |
| JANSKY_early_SCP_genes | -0.2596 | 0.0043 | -2.7665 | 0.006 | 0.0498 | -2.8377 | SCLCs | metastatic_vs_nonmetastatic_in_C1A |

**Supplementary Table 4.** IHC antibodies and antigen retrieval methods

| Antibody | Species | Distributor | Catalogue# | Dilution | Secondary | Antigen retrieval |
|---|---|---|---|---|---|---|
| CD3 (SP7) | Rabbit | Abcam | Ab16669 | 1:200 | anti-Rabbit (ImmPRESS Vector labs) | Citrate Buffer, pH6 |
| CD68 (514H12) | Mouse | Thermofisher Scientific | MA1-80133 | 1:100 | anti-Mouse (ImmPRESS Vector labs) | Tris EDTA, pH9 |
| CD206 | Rabbit | Abcam | Ab64693 | 1:10000 | anti-Rabbit(ImmPRESS Vector labs) | Citrate Buffer, pH6 |
| CD163 (MRQ-26) | Mouse | Millipore Sigma | CM163M14 | 1:200 | anti-Mouse (ImmPRESS Vector labs) | Tris EDTA, pH9 |
| S100 | Rabbit | Dako | Z3011 | 1:1000 | anti-Rabbit (ImmPRESS Vector labs) | Tris EDTA, pH9 |

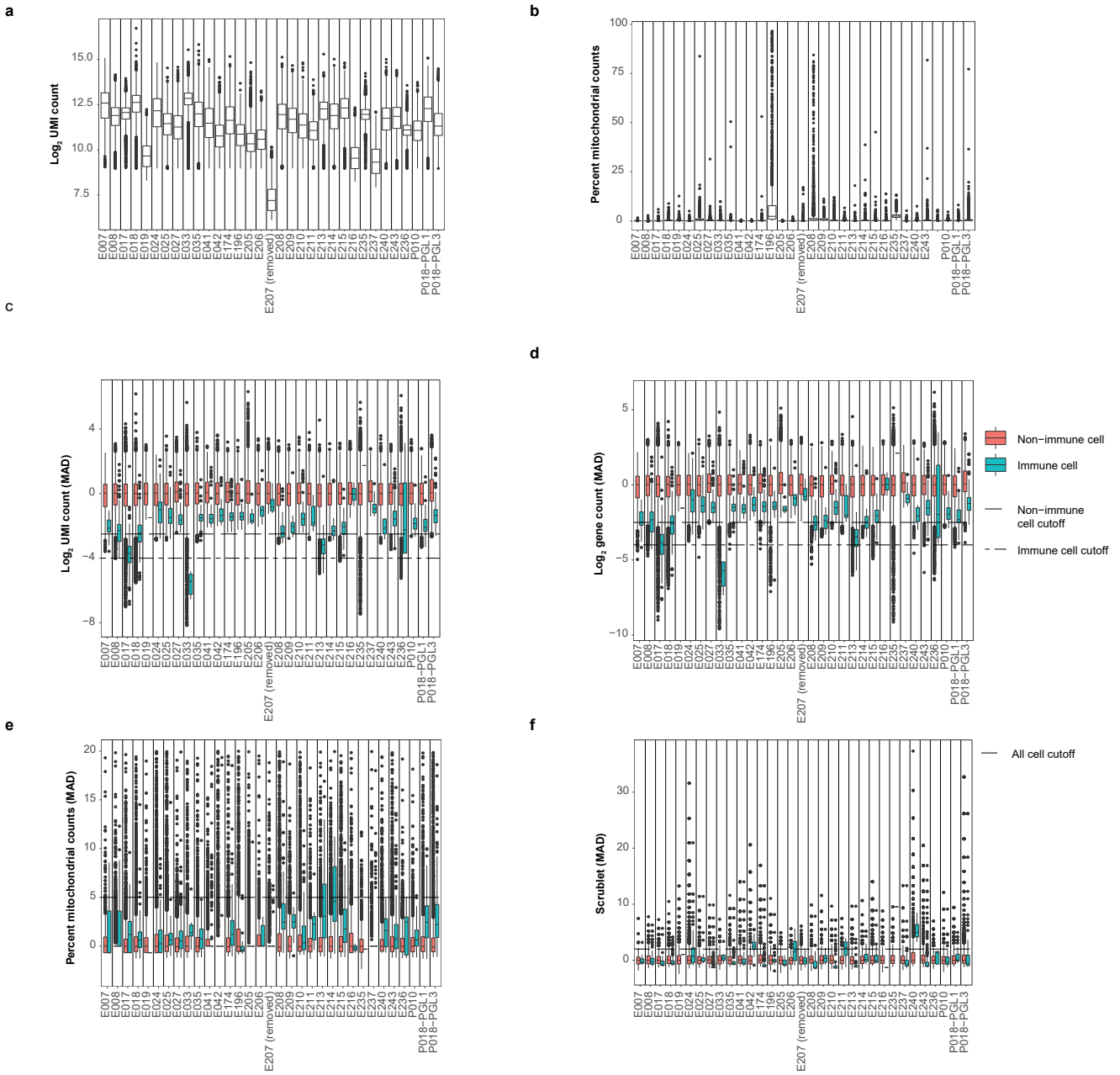


**Supplementary Figure 1.** QC and QC cutoffs of snRNA-Seq samples. **a**, $Log_2$ UMI counts of each sequenced sample (E207 was removed due to low library complexity). **b**, Per-nuclei percent mitochondrial read counts for each sample. Some samples displayed high global mitochondrial counts so an absolute filter threshold was not used. **c**, Median absolute deviation (MAD) $Log_2$ UMI counts for each sample, separated into non-monocyte-derived immune cell categories (based on scMatch) and otherwise per sample. A threshold of -4 was used for the immune cell group and -2.5 otherwise. **d**, MAD $Log_2$ gene counts for the same groups as (**c**). The same filter thresholds were used. **e**, MAD percent mitochondrial count values of each sample. Cells above 5 MADs were filtered. **f**, MAD Scrublet values. A threshold of 2 was chosen based on inspection of clusters showing intermediate gene expression and high average Scrublet scores. **a-f**, The lower and upper hinges of each boxplot correspond to the first and third quartiles, respectively, and the median value is marked. The whiskers extend from the hinges to the largest and smallest value no greater than 1.5 times the interquartile range above or below the upper and lower hinges, respectively. Values beyond the whisker extents are deemed outliers and are plotted individually. Number of samples=33; Number of cells per sample: E007=1040, E008=5214, E017=5540, E018=5177, E019=4534, E024=4902, E025=4295, E027=3943, E033=4162, E035=5190, E041=3493, E042=3154, E174=3987, E196=2856, E205=4111, E206=2962, E207=3432, E208=4105, E209=3374, E210=2952, E211=4435, E213=3617, E214=3706, E215=3787, E216=3230, E235=4140, E237=1596, E240=5519, E243=4672, E326=4717, P010=3653, P018-PGL1=4715, P018-PGL3=4729.

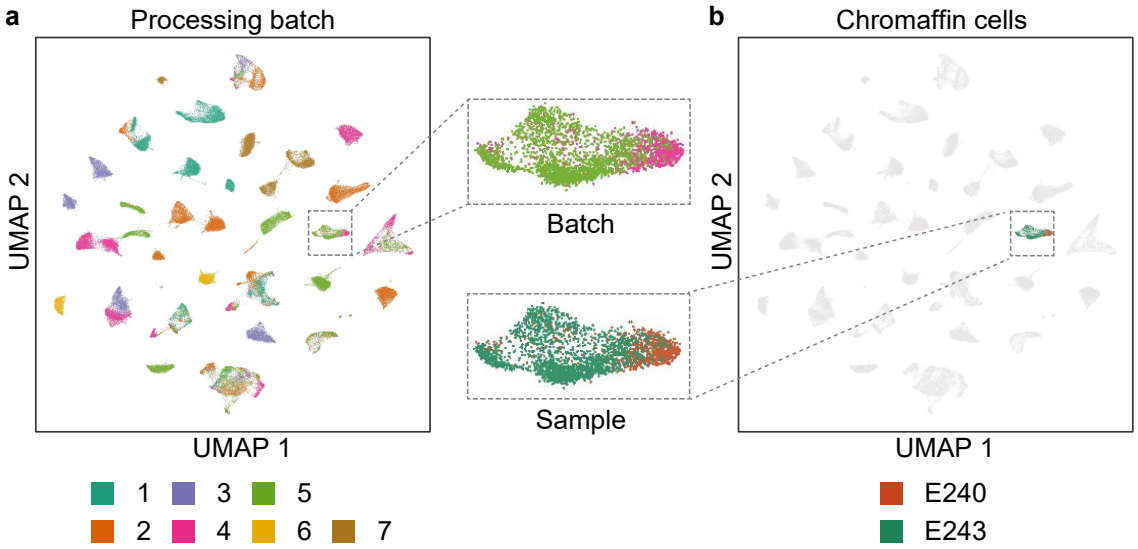


**Supplementary Figure 2**. UMAP projections for uncorrected PCPG snRNA-seq data show patient-specific clustering of PCPG tumor cells but not normal cells. **a**, UMAP colored by processing batch. **b**, The same UMAP as (a), colored by sample of origin, with cell types other than normal chromaffin cells colored grey.

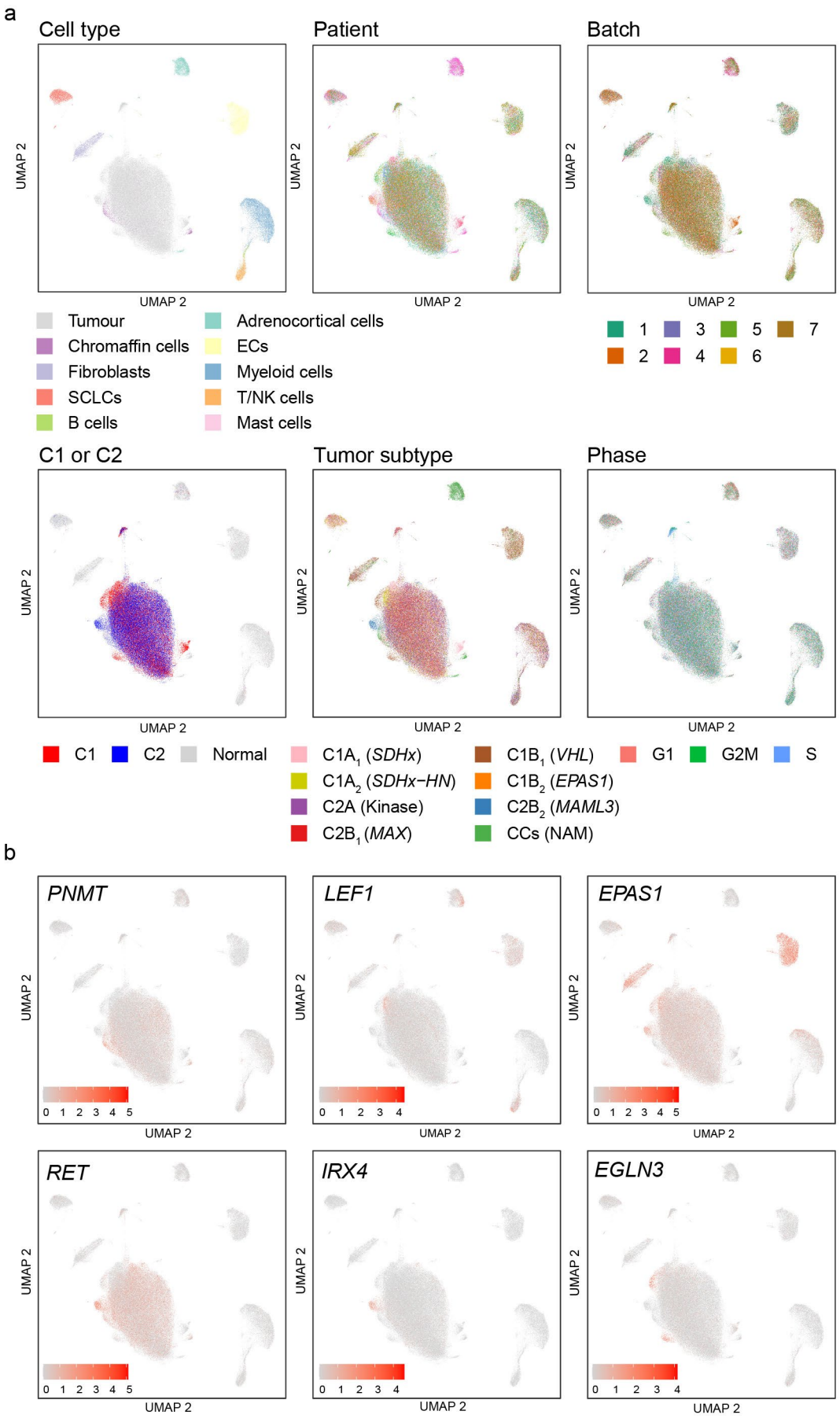


**Supplementary Figure 3**. Using Harmony batch correction to remove patient-specific effects in PCPG snRNA-seq. **a**, UMAP projections for batch-corrected PCPG snRNA-seq data, colored by different metadata as indicated by the plot subtitles. **b**, Feature plots of gene expression of cell type and tumor subtype marker genes.

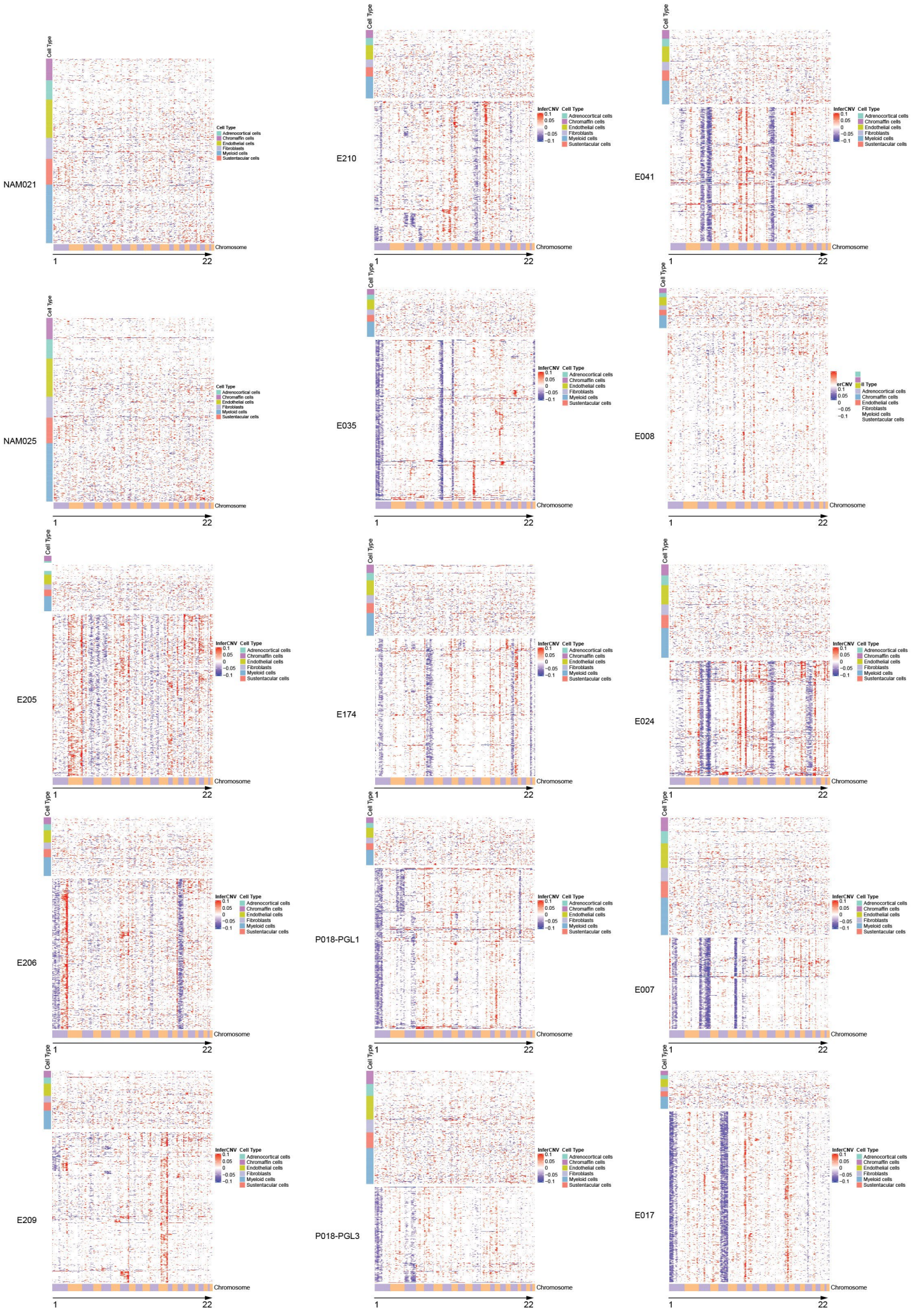
NAM021
E210
E041
NAM025
E035
E008
E205
E174
E024
E206
P018-PGL1
E007
E209
P018-PGL3
E017
Cell Type
Chromosome
InferCNV
Adrenocortical cells
Chromaffin cells
Endothelial cells
Fibroblasts
Myeloid cells
Sustentacular cells
1
22

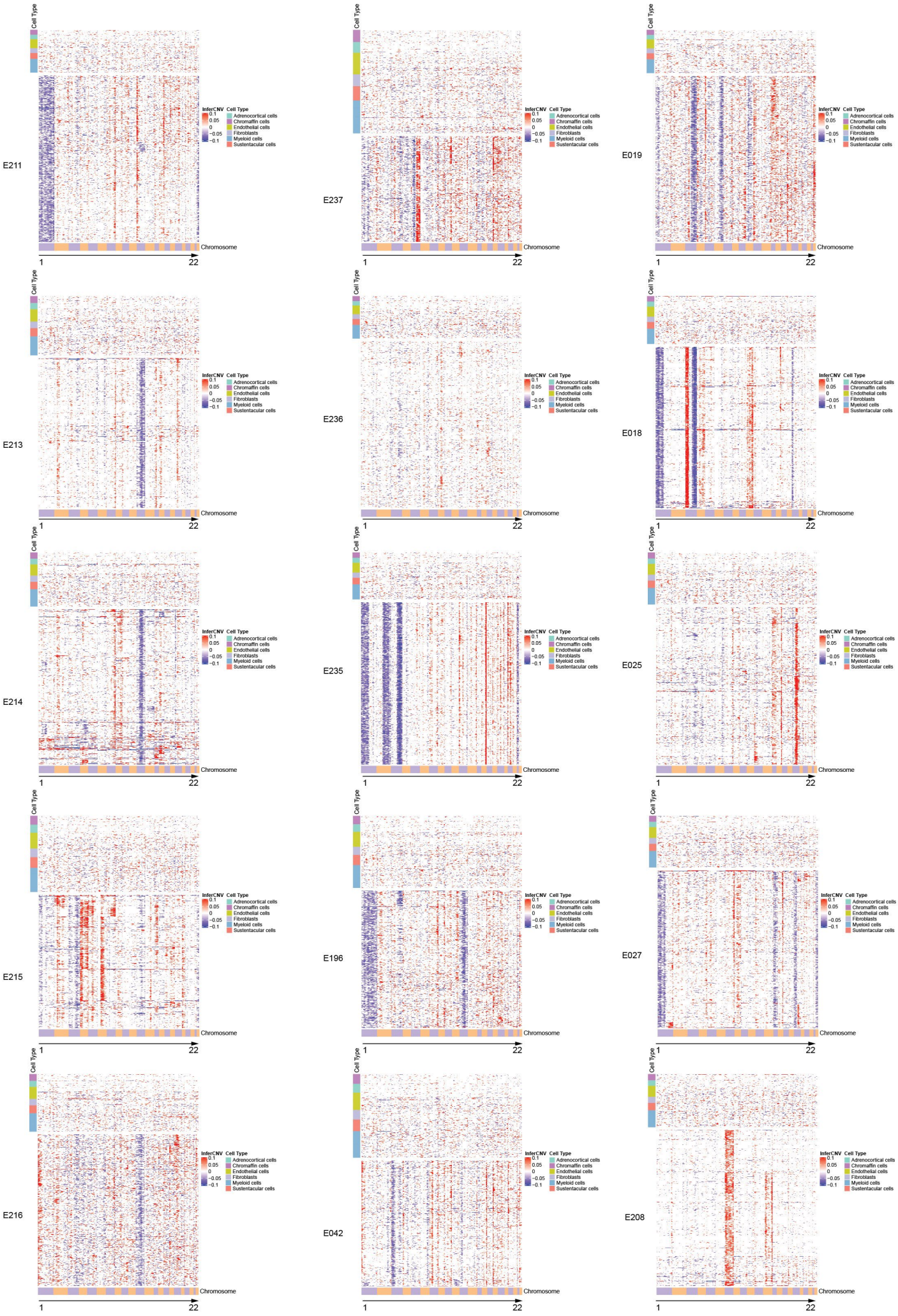
E211
E237
E019
E213
E236
E018
E214
E235
E025
E215
E196
E027
E216
E042
E208
Cell Type
Chromosome
1
22
InferCNV
0.1
0.05
0
−0.05
−0.1
Adrenocortical cells
Chromaffin cells
Endothelial cells
Fibroblasts
Myeloid cells
Sustentacular cells

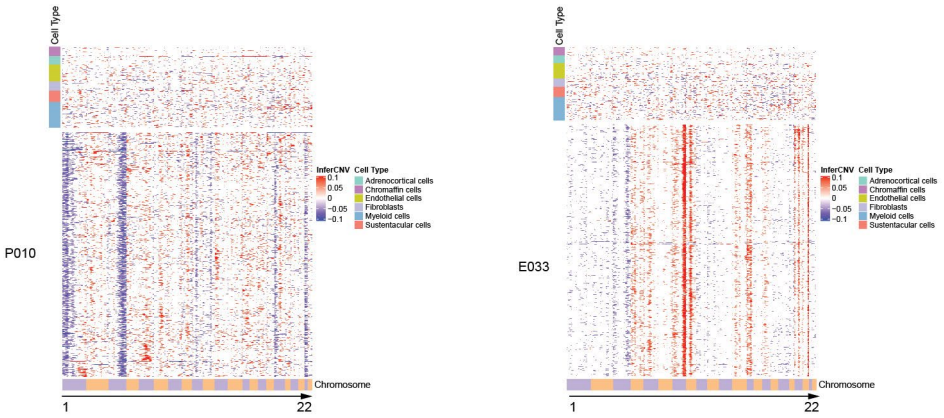


**Supplementary Figure 4.** Inference of copy-number in PCPG and normal adrenal snRNA-seq. Both NEO and non-NEO cell types are shown (bottom panel; tumor cells, top panel; non-neoplastic cell types from all tumors and NAM tissues).

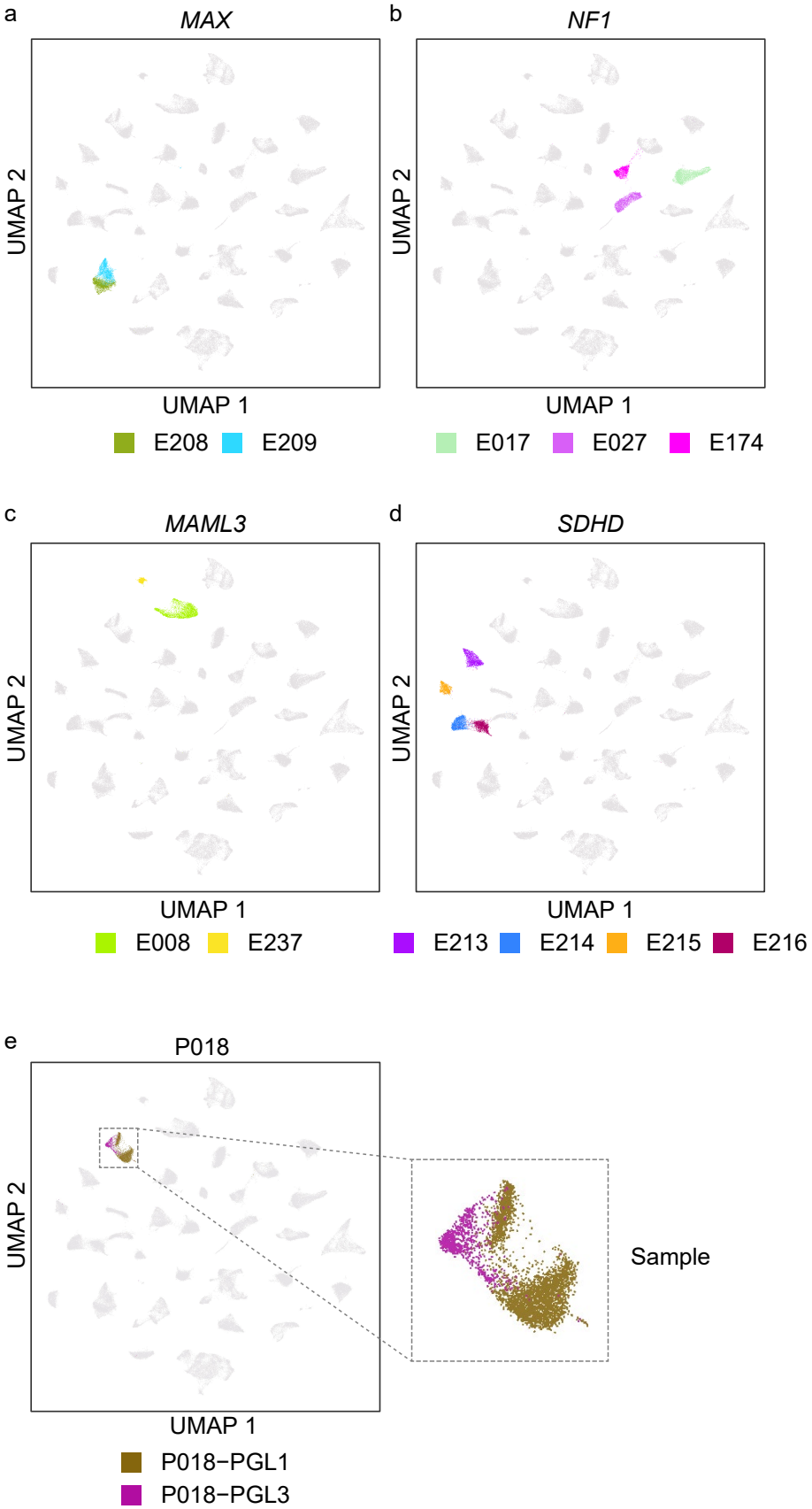


**Supplementary Figure 5.** UMAP projections for uncorrected PCPG snRNA-seq data show co-clustering of PCPG tumor samples based on PCPG driver mutations and tight synchronous primary PCPG tumors. **a-d**, UMAP projections each highlighting clustering of tumor nuclei for a specific tumor genotype. Nuclei from a single tumor genotype are colored according to sample of origin. Non-tumor nuclei and nuclei not belonging to the specified genotype are colored grey. **e**, UMAP highlighting tight co-clustering of synchronous primary PCPG samples collected from the same patient, tumor cells from patient P018 are colored according to tumor sample and cells from patients other than P018 are coloured grey.

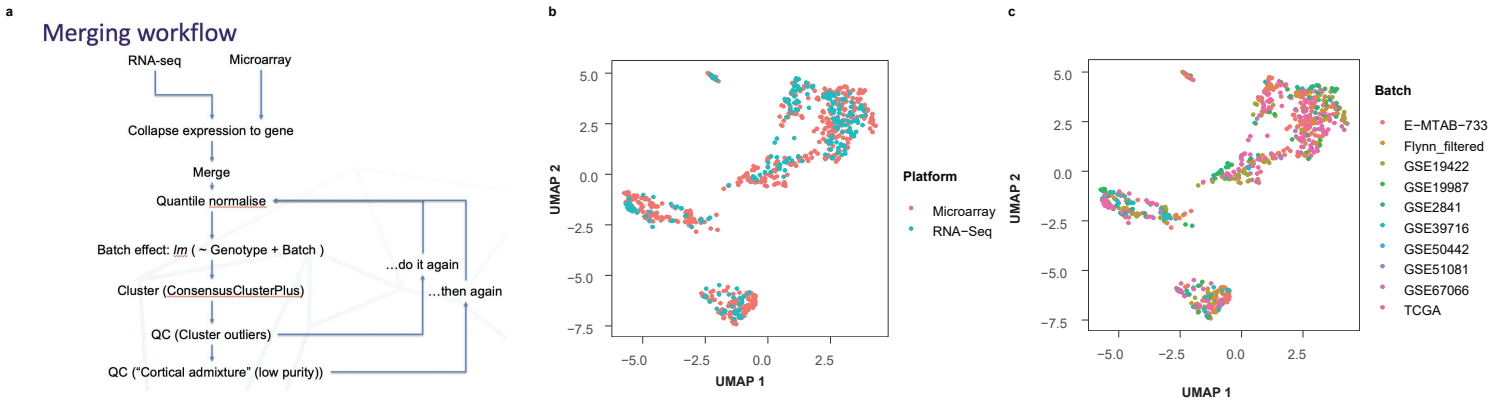


**Supplementary Figure 6.** Creation of the bulk RNA compendium **a**, Schematic description of data pooling and harmonization. Initial clustering attempts identified a cluster that was associated with datasets GSE19987 and GSE2841 but not of any particular genotypes. The cluster did not have a clear gene signature and had significantly higher than average normalized unscaled standard errors (NUSE), so these samples were deemed to be low-quality arrays and removed from the analysis before the merging process was repeated. A final consensus cluster number of nine was chosen based on the point at which the proportion of ambiguously clustered pairs stopped changing significantly. Additionally, a cluster associated with a normal cell gene signature and not any particular genotypes (C2C) was identified. Since this was a confounding factor in the batch effect removal model, the batch effect removal process was repeated a third time with samples initially assigned to cluster C2C to zero weight to improve performance. Two clusters associated with the kinase genotypes (C2A) were merged, yielding the final eight PCPG clusters. UMAPs with samples coloured by platform

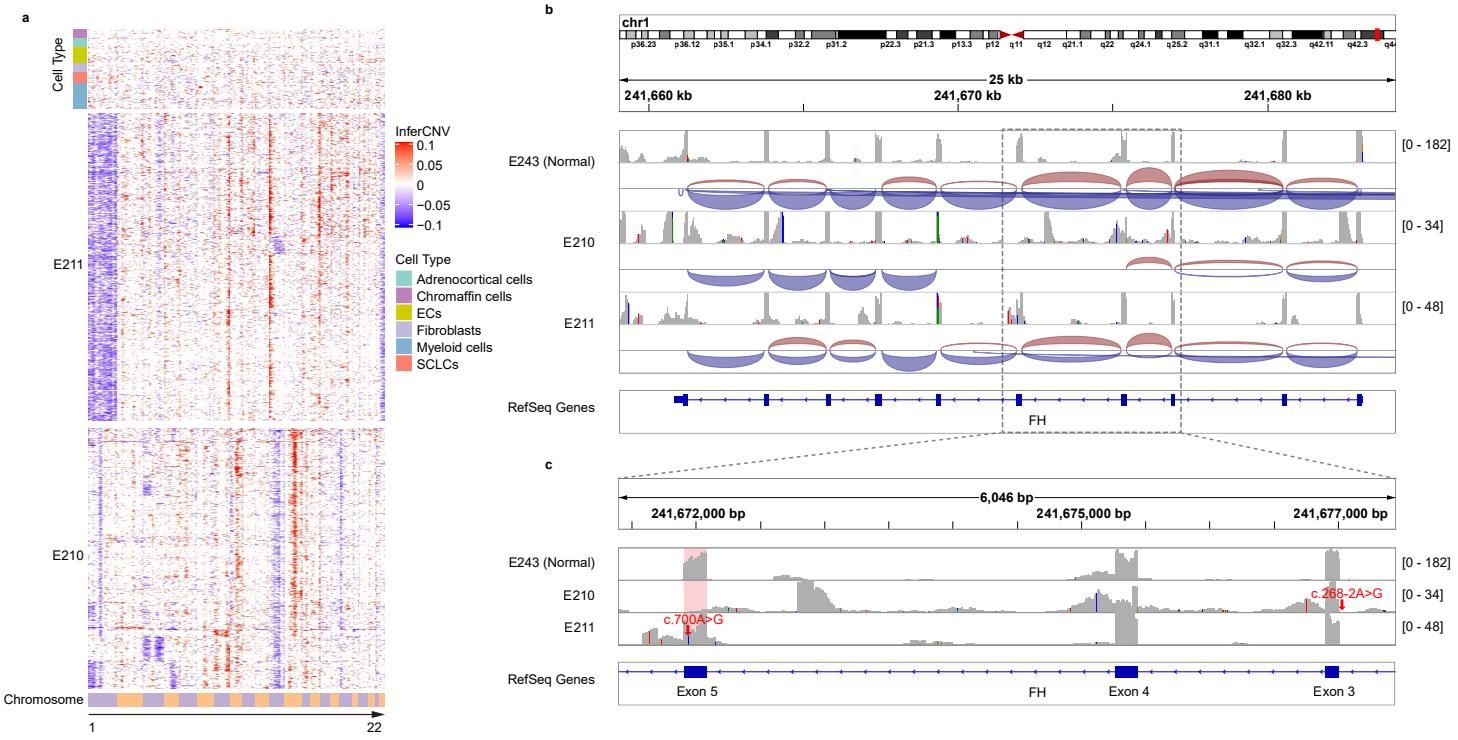


**Supplementary Figure 7.** snRNA-seq evidence for *FH* mutations in PCPG. a. Inferred CNV heatmaps for NEO cells for the *FH*-mutant samples (E210, E211) and normal cell types. b,c. Genome browser view of snRNA-seq read pileups for *FH* mutant samples and normal adrenal medulla control (E243). Reads from all cells (including NEO and normal cell types) are shown. b. snRNA-seq coverage for the entire *FH* gene, with sashimi plot illustrating splice junction. c. Zoomed-in coverage of mutations in *FH*. A c.268-2A>G mutation had previously been identified in E210 and this sample had evidence of disrupted splicing with reduced coverage at exon 5 (region highlighted in red). snRNA-seq reads confirmed presence of a c.700A>G mutation in E211. *FH* mutation positions are shown by

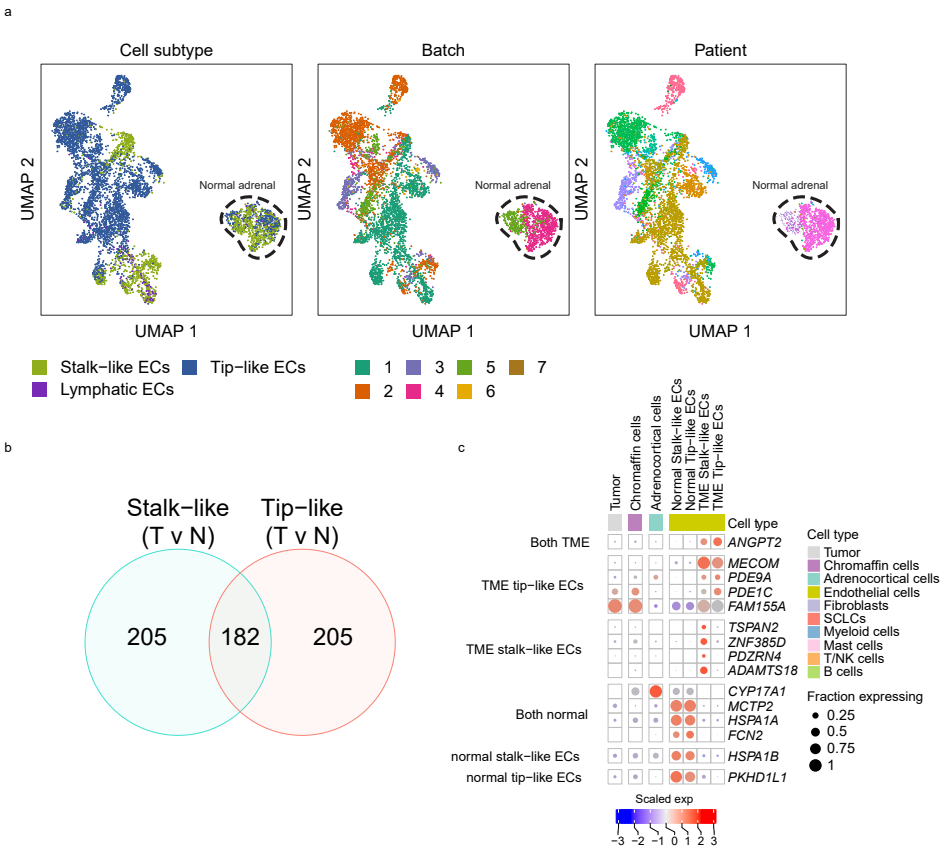


**Supplementary Figure 8.** Tumor-normal comparison within endothelial cell subsets. **a**, The same UMAP projection as shown in Figure 3d, colored by endothelial cell subtype, processing batch and patient. **b**, Venn-diagram showing the overlap between DEGs from comparisons between tumor-associated tip-like ECs (TME tip-like ECs) versus normal tip-like ECs, and tumor-associated stalk-like ECs (TME stalk-like ECs) versus normal stalk-like ECs (differential gene expression was decided using empirical Bayes moderated t-statistics, significant results were those with a Benjamini-Hochberg adjusted P-value < 0.05 and absolute $\log_2$FC > 0.5). **c**, Dotplot showing gene expression for top DEGs from the DE analyses in (b).

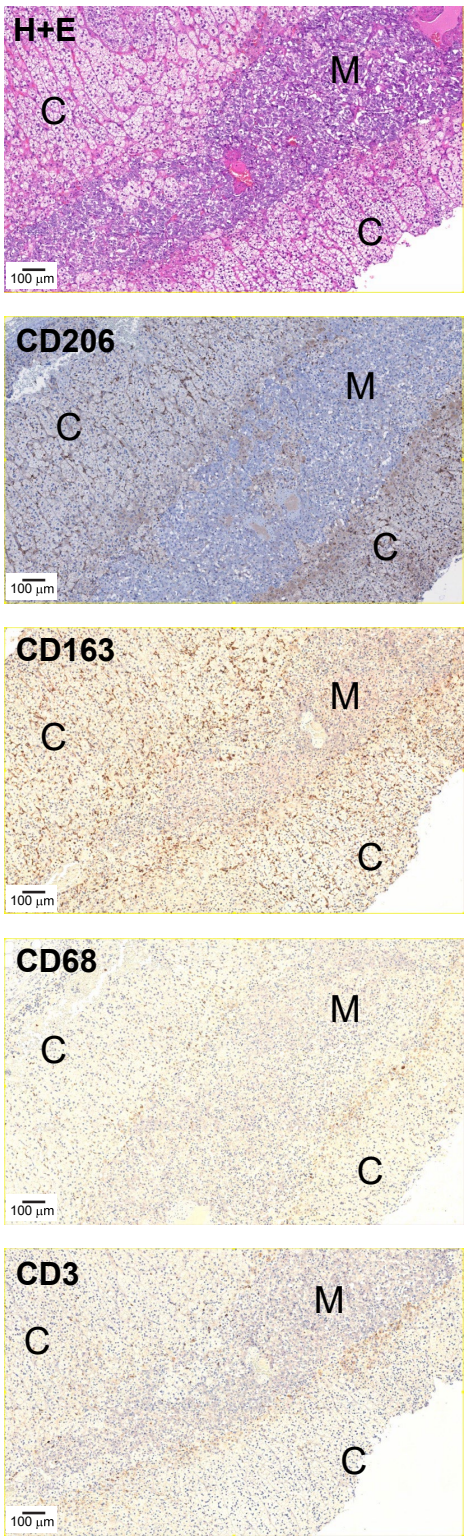


**Supplementary Figure 9.** Hematoxylin and eosin plus immunohistochemical staining of macrophage markers (CD206, CD168, CD68) and T cell marker (CD3) in a normal adrenal tissue (n=2, representative sections from a single sample shown). CD206+ and CD163+ cells were more numerous in the adrenal cortex compared to the medulla. Few CD68+ and CD3+ cells were observed in either the cortex or medulla regions. Scale bar indicates 100 micrometers.

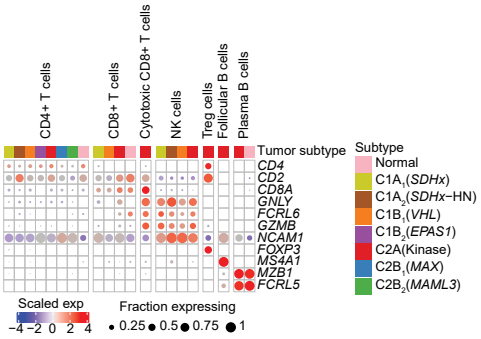


**Supplementary Figure 10.** Expression of lymphocyte marker genes in the immune component of PPGL. Dotplot illustrating snRNA-seq expression of lymphocyte marker genes. Dot color indicates the mean gene expression across all cells of a given cell-type within a given subtype, values are scaled and centered. Dot size indicates the proportion of cells of the indicated cell-type with detectable expression of the gene. PPGL subtypes with less than 20 cells representing an immune cell type are excluded from the plot.

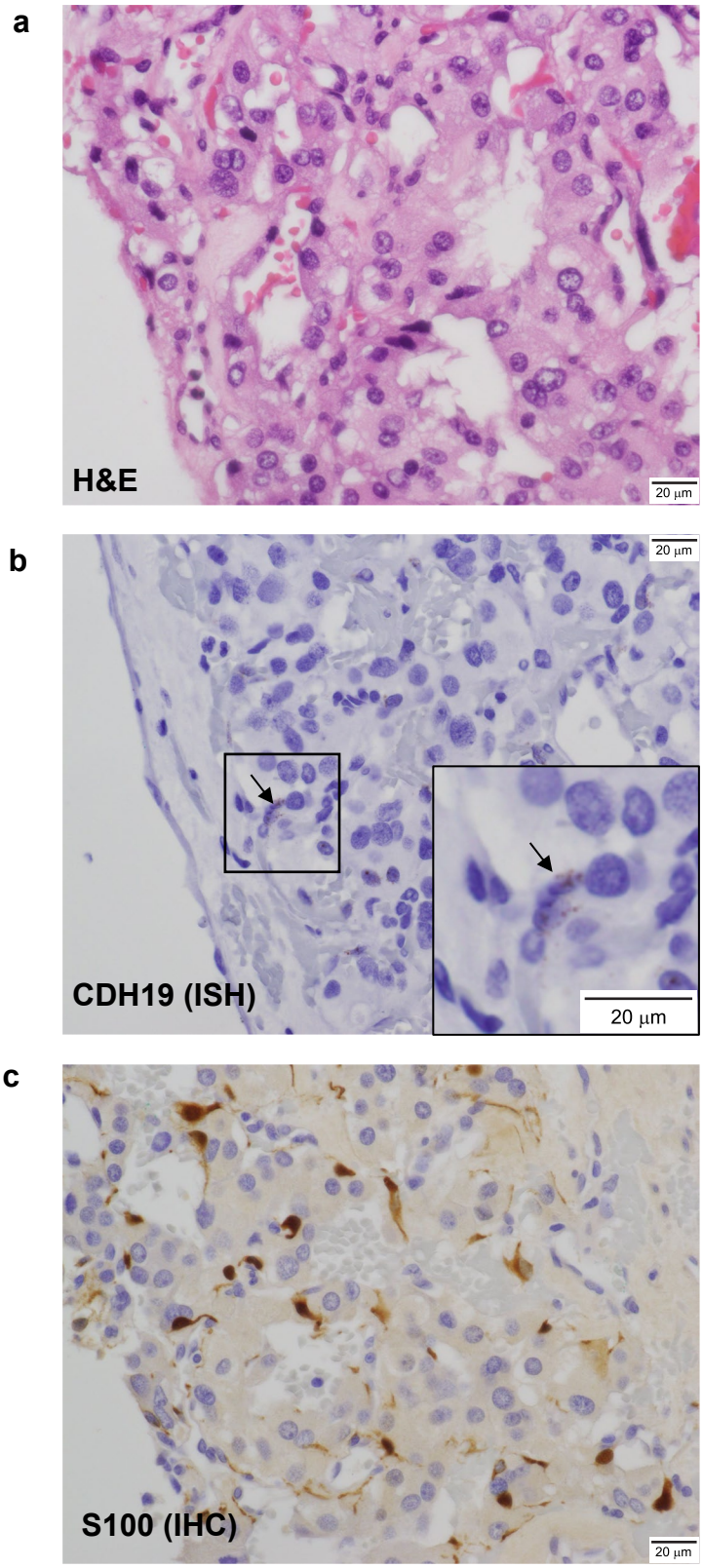


**Supplementary Figure 11.** CDH19 ISH (RNAscope) and S100 immunohistochemistry staining on tumor P018-PGL1. **a**, hematoxylin and eosin stained section (n=1). **b**, CDH19 ISH (n=1). **c**, S100 IHC (n=1). Scale bar indicates 20 micrometers.

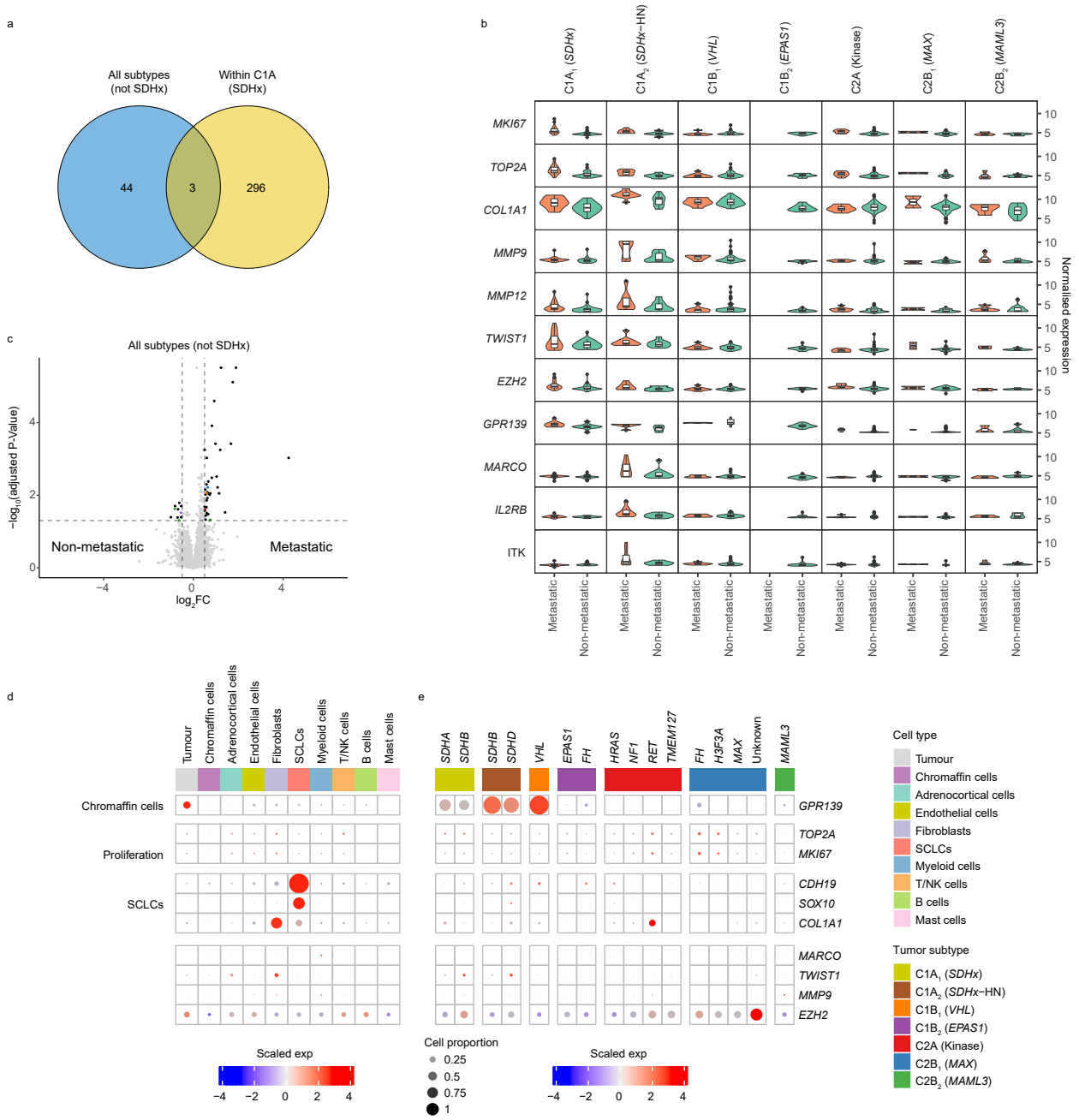


**Supplementary Figure 12.** Differential gene expression patterns in metastatic and non-metastatic PCPG. **a**, Venn-diagram illustrating the overlap between genes that were differentially expressed in metastatic vs non-metastatic PCPG across all subtypes other than C1A tumor, and genes that were differentially expressed in metastatic vs non-metastatic PCPG in just the C1A tumors (BH-adjusted P value < 0.05, log2FC > 0.5). **b**, Violin plots of gene expression for genes detected as differentially expressed, plotted individually for each tumor subtype (total samples: 382; samples per group: $C1A_1$-metastatic=23, $C1A_2$-metastatic=8, $C1B_1$-metastatic=8, C2A-metastatic=7, $C2B_1$-metastatic=2, $C2B_2$-metastatic=4, $C1A_1$-non-metastatic=31, $C1A_2$-non-metastatic=9, $C1B_1$-non-metastatic=69, $C1B_2$-non-metastatic=19, C2A-non-metastatic=145, $C2B_1$-non-metastatic=48, $C2B_2$-non-metastatic=9). The lower and upper hinges of each boxplot correspond to the first and third quartiles, respectively, and the median value is marked. The whiskers extend from the hinges to the largest and smallest value no greater than 1.5 times the interquartile range above or below the upper and lower hinges, respectively. Values beyond the whisker extents are deemed outliers and are plotted individually. **c**, Volcano plot indicating differentially expressed genes in the bulk RNA-seq cohort for metastatic vs non-metastatic PCPG within all subtypes other than the C1A SDHx subtypes. **d**,**e**, Dot plot describing snRNA-seq expression of genes that were detected as differentially expressed in the bulk RNA-seq comparison of metastatic vs non-metastatic PCPG in the C1A (SDHx) cluster tumors. Expression is shown in all normal cell types and aggregated tumor nuclei (d) and in all tumor nuclei aggregated by tumor genotype and subtype (e).